Squirming in a viscous fluid enclosed by a Brinkman medium

Herve Nganguia
Department of Mathematical and Computer Sciences, Indiana University of Pennsylvania, Indiana, Pennsylvania 15705, USA

Lailai Zhu
Department of Mechanical Engineering, National University of Singapore, Singapore 117575

D. Palaniappan
Department of Mathematics and Statistics, Texas A&M University, Corpus Christi, Texas 78412, USA

On Shun Pak
Department of Mechanical Engineering, Santa Clara University, Santa Clara, California 95053, USA

(Received 4 March 2020; accepted 27 May 2020; published 30 June 2020)

Cell motility plays important roles in a range of biological processes, such as reproduction and infections. Studies have hypothesized that the ulcer-causing bacterium *Helicobacter pylori* invades the gastric mucus layer lining the stomach by locally turning nearby gel into sol, thereby enhancing its locomotion through the biological barrier. In this work, we present a minimal theoretical model to investigate how heterogeneity created by a swimmer affects its own locomotion. As a generic locomotion model, we consider the swimming of a spherical squirmer in a purely viscous fluid pocket (representing the liquified or degelled region) surrounded by a Brinkman porous medium (representing the mucus gel). The use of the squirmer model enables an exact, analytical solution to this hydrodynamic problem. We obtain analytical expressions for the swimming speed, flow field, and power dissipation of the swimmer. Depending on the details of surface velocities and fluid properties, our results reveal the existence of a minimum threshold size of mucus gel that a swimmer needs to liquify in order to gain any enhancement in swimming speed. The threshold size can be as much as approximately 30% of the swimmer size. We contrast these predictions with results from previous models and highlight the significant role played by the details of surface actuations. In addition to their biological implications, these results could also inform the design of artificial microswimmers that can penetrate into biological gels for more effective drug delivery.

DOI: 10.1103/PhysRevE.101.063105

I. INTRODUCTION

Locomotion of microorganisms plays important roles in a wide range of biological processes, from swimming of spermatozoa in reproduction [1] to bacterial foraging and infections [2,3]. Many microorganisms use one or more appendages, called flagella and cilia, for propulsion [4,5]. Some eukaryotic cells swim by beating their flexible flagella, which is caused by the action of molecular motors within the flagellum. Ciliated microorganisms (e.g., *Paramecium* and *Volvox* [6]) are covered by arrays of cilia on their surfaces, which beat in coordinated manners to generate propulsion. Bacterial cells, on the other hand, utilize rotary motors embedded in the cell walls to rotate their passive, rigid helical flagella for swimming [4,7]. Taylor pioneered the hydrodynamic analysis of swimming microorganisms by modeling flagellar swimming of a spermatozoon as a waving sheet in Stokes flows [8]. The spherical squirmer model by Lighthill and Blake [9,10] for ciliary propulsion has also gained popularity as a generic locomotion model for different types of swimmers [11]. Extensive hydrodynamic analyses of different microorganisms in the past several decades have improved our general understanding of low-Reynolds-number locomotion [12–14], which has also informed the design of artificial microswimmers [15–18]. These synthetics possess vast potential for biomedical applications such as microsurgery and drug delivery [19–21].

Both biological and artificial microswimmers often need to traverse heterogenous biological environments with vastly varying properties. The capability to maintain robust locomotive capabilities across different media represents a major achievement of biological evolution and is essential for practical biomedical applications of artificial microwimmers. Interestingly, studies have hypothesized that some bacteria actively create heterogeneous geometries to enhance their locomotion. These include the local depletion of polymer concentration around rotating flagella of the bacterium *Escherichia coli* [22], and the invasion of the ulcer-causing bacterium *Helicobacter pylori* into the gastric mucus layer via local alternation of the surrounding mucus gel [23,24]. In this work, we focus on the latter example and consider a simple model to elucidate how heterogeneity created by the swimmer affects its propulsion performance. We also discuss the implications of our results

on the proposed mechanism of enhanced motility of *H. pylori* and the design of artificial microswimmers for drug delivery.

Different biological barriers defend the human body against the invasion of pathogens. These barriers include the mucus layers adherent to the epithelial surfaces of the stomach and intestinal tract, which hinder the penetration of pathogens into the host's tissues [25]. The mucus layer is a gel under acidic condition in the stomach, making it difficult for pathogens to penetrate. However, bacteria *H. pylori* have developed strategies to overcome the mucus barrier. The bacterium releases the urease enzyme to catalyze the hydrolysis of urea, which generates ammonia to locally neutralize the acidic environment. This local increase in pH induces a transition of the surrounding mucus from gel to sol [23,24]. Such a degelling process allows the bacterium to swim in a liquefied region (a fluid pocket) encompassed by the mucus gel. The enhanced motility of the bacterium in the liquefied or degelled region is hypothesized to be a plausible mechanism for *H. pylori* to move through the mucus barrier and cause infections that affect half of the world's population [26,27]. As a remark, these mucus barriers not only defend against invading pathogens but also drug carriers. The latter presents a major obstacle for more effective drug delivery. Inspired by the strategy employed by *H. pylori* to swim through the mucus barrier, artificial microswimmers with surface-immobilized urease have been developed to penetrate biological gels [28]. This biomimetic approach demonstrated the possibility to engineer microparticles that can actively modify their surrounding environment for enhanced mobility and thus more efficient drug delivery systems.

Mirbagheri and Fu [29] pioneered the theoretical analysis of the motility of *H. pylori* in the gastric mucus layer. They employed a two-dimensional waving sheet model to investigate the relation between the swimming speed and the size of the degelled region. The degelled region around the swimmer is modeled as a Newtonian fluid, which is bounded by the mucus gel, modeled as a Brinkman porous medium. Their analysis found that the size of the degelled region should be large relative to the size of the swimmer, for a self-consistent solution between the swimming problem and the mass transport of ammonia. More recently, Reigh and Lauga [30] presented a three-dimensional squirmer model swimming in a low-viscosity Newtonian fluid (degelled region), which is enclosed by another Newtonian fluid of a higher viscosity (mucus gel). An exact, analytical solution was obtained to this two-fluid problem, which accounts for the three-dimensional geometry and finite size of the swimmer. However, while it is hypothesized that *H. pylori* can enhance its locomotion by liquifying its surrounding medium, this two-fluid model for a squirmer does not predict an enhanced speed when the squirmer is immersed in the degelled region, regardless of the size of the degelled region. In this paper, we will demonstrate that by accounting for the porous structure of the mucus gel, we find swimming characteristics not observed in previous models. Our results generate a physical picture that is consistent with the benefits of degelation for enhanced locomotion.

This paper is organized as follows. We present the mathematical formulation of the problem in Sec. II, where the squirmer model (Sec. II A) and solutions to the governing equations in the liquified region and mucus gel (Sec. II B) are formulated. In Sec. III, we then calculate the swimming speed (Sec. III A), flow field, and power dissipation (Sec. III B) of the swimmer. We then compare these results with those of previous models and discuss their implications, before some concluding remarks in Sec. IV.

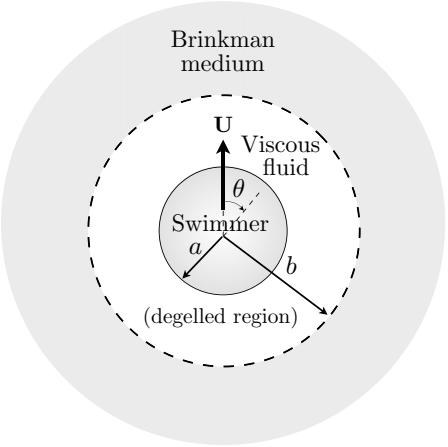

FIG. 1. Setup of a minimal model for a spherical swimmer in a viscous solution (representing the liquified or degelled region) enclosed by a Brinkman porous medium (representing the mucus gel). The swimmer of radius a propels at a speed $\mathbf{U}$ via a distribution of surface velocities. The boundary of the degelled region is at a distance b from the center of the swimmer, with $\lambda = b/a$.

II. FORMULATION

A. The squirmer model

We model the swimmer as a spherical squirmer of radius a (Fig. 1). The squirmer model was first studied by Lighthill and Blake [9,10] as an idealized model for ciliary propulsion. The beating of cilia is represented by surface velocities on the spherical cell body. We follow this approach and consider a squirmer with prescribed, time-independent velocities decomposed into a series of the form at the surface ($r = a$) as [11]

$$\mathbf{u}_{sq} = \sum_{n=1}^{\infty} B_n V_n(\cos\theta)\mathbf{e}_\theta, \tag{1}$$

where $V_n(\cos\theta) = -2P_n^1(\cos\theta)/[n(n+1)]$ and $P_n^1(\cos\theta)$ are the associated Legendre polynomials of the first kind, with θ being the polar angle measured with the axis of symmetry and r being the distance from the center of the squirmer (Fig. 1). The coefficients B_n are related to Stokes singularity solutions. In Stokes flow, the B_1 mode corresponds to a source dipole and is the only mode contributing to swimming. The B_2 mode corresponds to a Stokes force dipole and is the slowest decaying spatial mode in the far field. Therefore, often only the first two modes, B_1 and B_2, of the series are considered in locomotion problems [11] and their relative signs can be adjusted to represent different types of swimmers: $B_2/B_1 > 0$ represents a puller, which generates thrust from its front end (e.g., the alga *Chlamydomonas*), whereas $B_2/B_1 < 0$ represents a pusher, which generates propulsion from its rear part (e.g., the bacterium *Escherichia coli*), and the $B_2/B_1 = 0$ case corresponds to a neutral squirmer. We will therefore focus our analysis

on the first two swimming modes and set $B_n = 0$ for $n > 2$. For its simplicity and elegance, the squirmer model has been extensively employed to probe different complexities that can arise in locomotion in practical and biological scenarios [11], including nutrient uptake [31–34], confinement [35–42] and inertial [43–45] effects, complex rheology [46–56], and collective behaviors [57–62], among others [63–66].

We consider in the main text squirmers with tangential surface velocities described by Eq. (1), which are more commonly studied in the literature [11]. Results on squirmers with radial surface velocities can be obtained in the same manner and are presented in Appendix A for comparison with the tangential case.

B. The Stokes-Brinkman model

The degelled region immediately adjacent to the squirmer is modeled as a purely viscous fluid, governed by the Stokes equation,

$$-\nabla p_S + \mu\nabla^2\mathbf{u}_S = \mathbf{0}, \tag{2}$$

for an incompressible flow ($\nabla\cdot\mathbf{u}_S = 0$), where μ is the fluid viscosity, and $\mathbf{u}_S$ and p_S represent the velocity and pressure fields in the degelled region, the annulus $a \leqslant r \leqslant b$. This fluid pocket is surrounded by the mucus gel, which is modeled as a Brinkman medium [29,67] and an incompressible flow ($\nabla\cdot\mathbf{u}_B = 0$). The Brinkman equation

$$-\nabla p_B + \mu\nabla^2\mathbf{u}_B - \mu\alpha^2\mathbf{u}_B = \mathbf{0} \tag{3}$$

includes the additional hydrodynamic resistance $-\mu\alpha^2\mathbf{u}_B$ due to the network of stationary obstacles. Here, α^{-2} is the permeability, and $\mathbf{u}_B$ and p_B are the average velocity and pressure fields, respectively. The Brinkman equation was introduced as a phenomenological model, but its validity at low particle volume fraction was established by proper averaging methods [68–71]. Even for moderately concentrated porous media, the Brinkman equation is still effective in capturing the qualitative behavior [72]. This effective medium approach via the Brinkman equation has been applied to study locomotion problems in porous media in recent studies [29,73–78].

We nondimensionalize the problem as follows: Velocities are scaled by the first mode B_1, and lengths are scaled by the squirmer radius a. The dimensionless size of the degelled region is hence characterized by $\lambda = b/a$, while stresses and pressure are scaled by $\mu B_1/a$. The dimensionless surface velocities in Eq. (1) hence become

$$\tilde{\mathbf{u}}_{sq} = \sum_{n=1}^{\infty}\beta_n V_n(\cos\theta)\mathbf{e}_\theta, \tag{4}$$

where the ratio $\beta_n = B_n/B_1$ and we focus on only the first two swimming modes by setting $\beta_n = 0$ for $n > 2$.

In dimensionless forms, the Stokes equation, which governs the flow in the degelled region ($1 < \tilde{r} < \lambda$), is given by

$$-\nabla\tilde{p}_S + \nabla^2\tilde{\mathbf{u}}_S = \mathbf{0}, \tag{5}$$

and the Brinkman equation, which governs the flow in the mucus gel ($\tilde{r} > \lambda$), is given by

$$-\nabla\tilde{p}_B + \nabla^2\tilde{\mathbf{u}}_B - \delta^2\tilde{\mathbf{u}}_B = \mathbf{0}. \tag{6}$$

Here $\delta = a\alpha$ is the dimensionless resistance in the Brinkman medium, which depends on the ratio of the squirmer radius a to the Brinkman screening length α^{-1}. Hereafter, we drop the tildes for simplicity and refer only to dimensionless variables unless otherwise stated.

In the laboratory frame, the flow velocity in the far field decays as

$$\mathbf{u}_B(r\to\infty) = \mathbf{0}, \tag{7}$$

and on the squirmer surface as

$$\mathbf{u}_S(r=1) = \mathbf{U} + \mathbf{u}_{sq}, \tag{8}$$

where $\mathbf{U}$ is the unknown swimming speed of the squirmer due to the squirming motion $\mathbf{u}_{sq}$ in Eq. (4).

At the interface between the viscous fluid and the Brinkman medium, $r = \lambda$, we maintain the continuity of the velocity and traction [29,79,80]

$$\mathbf{u}_S = \mathbf{u}_B, \qquad \mathbf{T}_S\cdot\mathbf{n} = \mathbf{T}_B\cdot\mathbf{n}, \tag{9}$$

where $\mathbf{T}_j = -p_j\mathbf{I} + \dot{\boldsymbol{\gamma}}_j$, with $j = S, B$ denoting the stress in the Stokes and Brinkman domains respectively, and $\mathbf{n}$ and $\dot{\boldsymbol{\gamma}}$, respectively, denote the unit normal vector and rate-of-strain tensor.

The solution to the Stokes equation, Eq. (5), for this axisymmetric problem can be obtained by a stream function formulation or directly given by Lamb's general solution [30,81] for the velocity field $\mathbf{u}_S = u_S\mathbf{e}_r + v_S\mathbf{e}_\theta$ as

$$u_S = \sum_{n=0}^{\infty}\left(O_n r^{n+1} + Q_n r^{n-1} + \frac{R_n}{r^n} + \frac{S_n}{r^{n+2}}\right)P_n(\cos\theta), \tag{10}$$

$$v_S = \sum_{n=1}^{\infty}\left(-\frac{n+3}{2}O_n r^{n+1} - \frac{n+1}{2}Q_n r^{n-1} + \frac{n-2}{2}\frac{R_n}{r^n} + \frac{n}{2}\frac{S_n}{r^{n+2}}\right)V_n(\cos\theta), \tag{11}$$

where O_n, Q_n, R_n, and S_n are unknown coefficients to be determined by boundary conditions.

We obtain the solution to the Brinkman equation, Eq. (6), by the stream function formulation, where

$$u_B = \frac{1}{r^2\sin\theta}\frac{\partial\psi_B}{\partial\theta}, \qquad v_B = -\frac{1}{r\sin\theta}\frac{\partial\psi_B}{\partial r}. \tag{12}$$

The stream function ψ_B can be obtained via separation of variables as [77,82,83]

$$\psi_B = \sin\theta\sum_{n=0}^{\infty}F_n(r)P_n^1(\cos\theta), \tag{13}$$

where

$$F_n(r) = T_n r^{-n} + V_n r^{n+1} + \frac{r^{1/2}}{\delta^2}[Z_n I_{n+1/2}(\delta r) + W_n K_{n+1/2}(\delta r)], \tag{14}$$

and $I_{n+1/2}(\delta r)$ and $K_{n+1/2}(\delta r)$ are, respectively, the modified Bessel functions of the first and second kinds. The flow in the far field decays to zero in the laboratory frame (7), which demands the growing terms in Eq. (14) to vanish, i.e., $V_n = Z_n = 0$ for $n \geqslant 1$. The remaining coefficients, T_n and W_n, combined with O_n, Q_n, R_n, and S_n from the Stokes solutions in

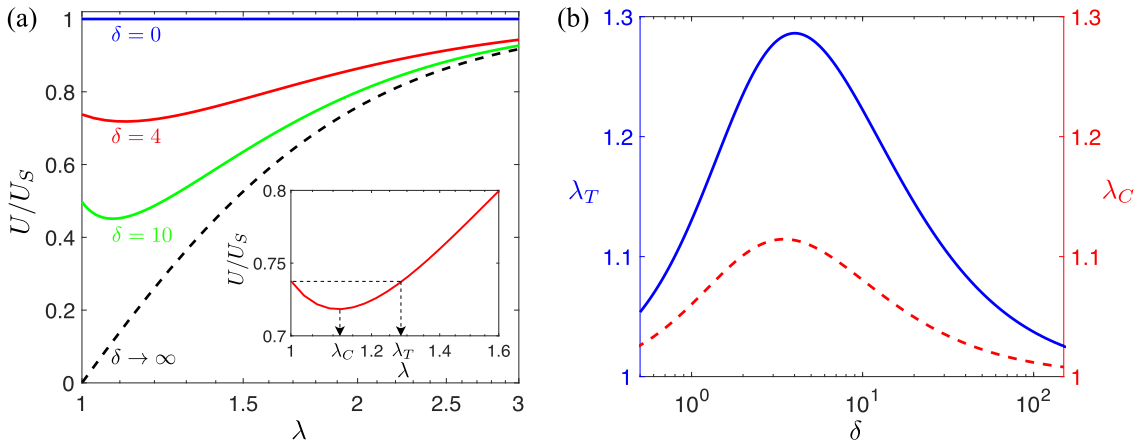

FIG. 2. (a) Swimming speed of a squirmer U with tangential surface velocities, normalized by its speed in the Stokes limit U_S, as a function of the size of the degelled region λ at different values of resistance δ. Inset: for a given resistance (shown results for $\delta = 4$), the swimming speed displays a local minimum at the critical size of the degelled region λ_C. The swimmer needs to liquify a minimum threshold size λ_T in order to gain any enhancement in speed. (b) The value of the critical size of the degelled region λ_C (red dotted line, right axis) and the threshold size λ_T (blue line, left axis) as a function of resistance δ.

Eqs. (10) and (11) to form a total of six unknowns, which can be obtained by solving a system of six equations given by the boundary conditions at the surface of the squirmer [Eq. (8)] and at the interface between the Stokes and Brinkman domains [Eq. (9)].

Upon applying the boundary conditions, we obtain the velocity and pressure fields for a two-mode squirmer, $\mathbf{u}_{sq} = [\sin\theta + (\beta_2/2)\sin 2\theta]\mathbf{e}_\theta$, in the Stokes domain (degelled region, $1 < r < \lambda$) as

$$u_S = \left(O_1 r^2 + Q_1 + \frac{R_1}{r} + \frac{S_1}{r^3} + U\right)\cos\theta + \frac{\beta_2}{4}\left(O_2 r^3 + Q_2 r + \frac{R_2}{r^2} + \frac{S_2}{r^4}\right)(1 + 3\cos 2\theta), \quad (15)$$

$$v_S = \left(-2O_1 r^2 - Q_1 - \frac{R_1}{2r} + \frac{S_1}{2r^3} - U\right)\sin\theta + \frac{\beta_2}{2}\left(-\frac{5}{2}O_2 r^3 - \frac{3}{2}Q_2 r + \frac{S_2}{r^4}\right)\sin 2\theta, \quad (16)$$

$$p_S = \left(10O_1 r + \frac{R_1}{r^2}\right)\cos\theta + \beta_2\left(\frac{7}{4}O_2 r^2 + \frac{R_2}{2r^3}\right)(1 + 3\cos 2\theta), \quad (17)$$

where the expressions for coefficients O_n, Q_n, R_n, and S_n for $n = 1, 2$ are given in Appendix B. The corresponding velocity and pressure fields in the Brinkman domain (mucus gel, $r > \lambda$) are given by

$$u_B = \left[\frac{2T_1}{r^3} + \frac{\sqrt{2\pi}W_1 e^{-r\delta}(1 + r\delta)}{r^3\delta^{7/2}}\right]\cos\theta + \beta_2\left[\frac{T_2}{2r^4} + \frac{\sqrt{2\pi}W_2 e^{-r\delta}(3 + 3r\delta + r^2\delta^2)}{4r^4\delta^{9/2}}\right] \times (1 + 3\cos 2\theta), \quad (18)$$

$$v_B = \left[\frac{T_1}{r^3} + \frac{\sqrt{2\pi}W_1 e^{-r\delta}(1 + r\delta + r^2\delta^2)}{2r^3\delta^{7/2}}\right]\sin\theta + \beta_2\left[\frac{T_2}{r^4} + \frac{\sqrt{2\pi}W_2 e^{-r\delta}(6 + 6r\delta + 3r^2\delta^2 + r^3\delta^3)}{4r^4\delta^{9/2}}\right] \times \sin 2\theta, \quad (19)$$

$$p_B = \frac{T_1\delta^2}{r^2}\cos\theta + \beta_2\frac{T_2\delta^2}{6r^3}(1 + 3\cos 2\theta), \quad (20)$$

where the expressions for coefficients T_n and W_n for $n = 1, 2$ are given in Appendix B. The above flow fields are determined up to the unknown swimming speed U along the axis of symmetry.

III. RESULTS AND DISCUSSION

In this section, we employ the solutions obtained in the Stokes [Eqs. (15)–(17)] and Brinkman [Eqs. (18)–(20)] domains to calculate the unknown swimming speed of the squirmer U in Sec. III A and its surrounding flow field $\mathbf{u}$ and power dissipation $\mathcal{P}$ in Sec. III B. We will contrast our findings with results from previous studies [29,30] and discuss their implications in terms of cell motility and design of artificial microswimmers.

A. Propulsion speed

To calculate the unknown swimming speed U, we enforce the force-free condition on the squirmer,

$$\int_S \mathbf{T}_S \cdot \mathbf{n}\, dS = \mathbf{0}, \quad (21)$$

where the stress on the squirmer surface $\mathbf{T}_S$ are determined by the velocity and pressure fields in Eqs. (15)–(20). The

swimming speed is obtained as

$$U = U_S - \frac{2\delta^2}{\mathcal{B}} - \frac{\delta^2(\lambda^2-1)(3+\lambda\delta)}{\mathcal{B}}, \tag{22}$$

where

$$\mathcal{B} = 3\left[(9+9\lambda\delta+\lambda^2\delta^2)\lambda^3 + \frac{\delta^2}{5}(\lambda^5-1)(1+\lambda\delta)\right]. \tag{23}$$

We first reduce our results to previously known limits. In the limit of $\delta = 0$ (or $\lambda \to \infty$), the outer region becomes a purely viscous fluid, and hence the swimming speed reduces to that in Stokes flow [9,10], i.e., $U_S = 2/3$. In the limit $\lambda = 1$, the third term on the right-hand side of Eq. (22) vanishes, and the expression reduces to the swimming speed of a squirmer in a Brinkman medium [73,77], $U = U_S[1 - \delta^2/(9+9\delta+\delta^2)]$. Finally, we consider the high resistance limit $\delta \to \infty$, where the expression reduces to $U = (2\lambda^5 - 5\lambda^2 + 3)/3(\lambda^5 - 1)$, agreeing with recent results obtained for a rigidly bounded flow [30].

It is clear from Eq. (22) that, for any finite size of the degelled region ($\lambda > 1$), the swimming speed of a squirmer with tangential surface velocities is always smaller than the speed in a purely viscous fluid ($U/U_S < 1$). Owning to the third term in the right-hand side of Eq. (22), the swimming speed varies nonmonotonically with the size of the degelled region [Fig. 2(a)]. As the degelled region expands (increasing λ), the swimming speed initially decreases for small λ, attaining a minimum speed at a critical size of the degelled region λ_C [see Fig. 2(a) inset for schematic illustration and Fig. 2(b) for the value]. As the size of the degelled region continues to expand, the speed of the swimmer increases and attains values higher than the speed when there is no degelation ($\lambda = 1$) when $\lambda > \lambda_T$ [see Fig. 2(a) inset]. This nonmonotonic behavior implies that as a biological or artificial swimmer attempts to degel the mucus layer to enhance its locomotion, there exists a minimum threshold of the size of the degelled region, λ_T, that the swimmer needs to surpass in order to achieve any enhancement in swimming speed. Below this threshold, the degelation could indeed hinder the swimmer's locomotion. In Fig. 2(b), we plot the magnitude of this threshold λ_T at varying values of δ; for $\delta = 4$, a swimmer needs to liquify as much as approximately 30% of its swimmer size to gain any enhancement in speed by degelation.

We contrast the above results with those by previous models [29,30]. While nonmonotonic variations of the propulsion speed were observed in previous models, they occur in qualitatively different manners. According to the results of a two-dimensional swimming sheet [29], the model predicts that (1) any size of confinement by the Brinkman medium leads to higher swimming speeds compared with that in a purely viscous fluid ($U/U_S > 1$), (2) local maxima instead of local minima in propulsion speed occur as the size of the degelled region varies, and (3) as the size of the degelled region increases beyond a threshold, the swimmer will have a lower speed compared with the case without any degelation ($\lambda = 1$). We argue that these qualitatively different characteristics between the waving sheet and the spherical squirmer models do not stem from the difference in spatial dimensionality of the setups. Instead, we attribute the difference to details of the swimming gaits. As a demonstration, we show that when radial surface velocities are prescribed on the spherical squirmer surface (see Appendix A), we obtain swimming characteristics similar to those of the waving sheet model described above (Fig. 3).

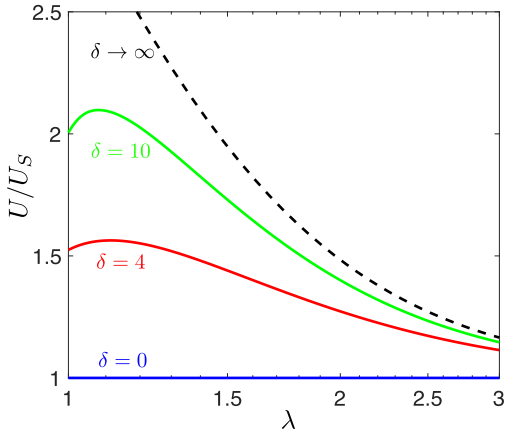

FIG. 3. Swimming speed U of a squirmer with radial surface velocities, normalized by its speed in the Stokes limit U_S, as a function of the size of of the degelled region λ with different values of resistance δ. The swimming speed displays local maxima as the size of the degelled region varies. In contrast to the case of a squirmer with tangential surface velocities (Fig. 2), as the size of the degelled region increases beyond certain thresholds, the swimmer experiences speed reduction compared with the case without any degelation ($\lambda = 1$).

The aforementioned results suggest that the details of swimming gaits could lead to different biological implications and design principles for artificial swimmers in terms of the benefits of degelation. While a squirmer with tangential surface velocities should strive to degel as much as possible (at least surpass the minimum threshold) to enhance its propulsion speed, a squirmer with radial surface velocities should only degel within a certain range beyond which a speed reduction occurs (Fig. 3). Reigh and Lauga [30] considered a spherical squirmer model as well but they modeled the outer mucus gel as a fluid with a higher viscosity, instead of a porous medium with additional resistance. While nonmonotonic variations in swimming also occur, their model predicts that the swimmer does not gain any speed enhancement from degelation, regardless of the size of the degelled region. Therefore, by modeling the mucus gel with additional resistance in a Brinkman medium, predictions from our model provide a plausible physical picture consistent with the strategy employed by *H. pylori* to enhance locomotion by liquifying its surrounding mucus gel.

B. Flow decay and power dissipation

The flow surrounding the swimmer is obtained by substituting the resultant propulsion speed, Eq. (22), into the solution in the Stokes [Eqs. (15)–(17)] and Brinkman [Eqs. (18)–(20)] domains. We examine the characteristics of flow decay in this Stokes-Brinkman system for a neutral squirmer [$\beta_2 = 0$, Fig. 4(a)] and a pusher-puller [$\beta_2 = \pm 1$, Fig. 4(b)]. As a comparison, we display a homogenous case where the resistance in the Brinkman medium vanishes ($\delta = 0$, dashed

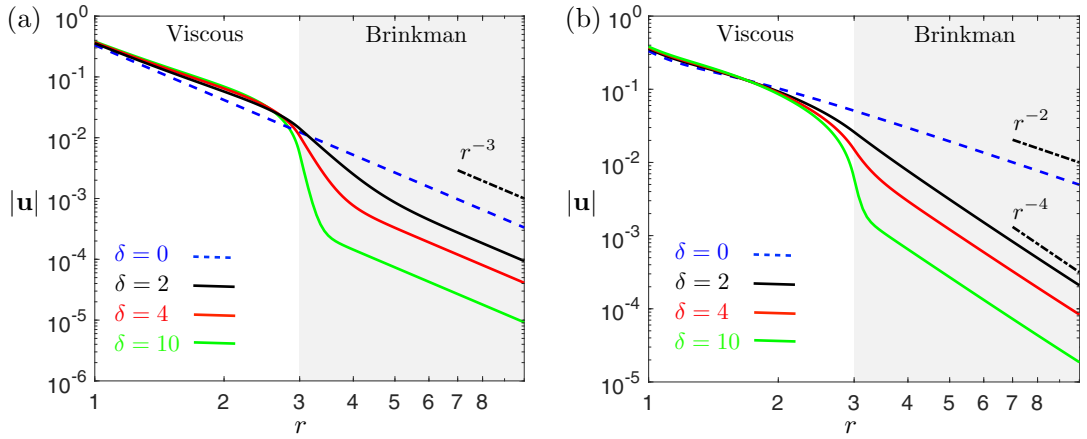

FIG. 4. The decay of the magnitude of flow velocity $|\mathbf{u}|$ around a (a) neutral squirmer ($\beta_2 = 0$) and (b) a pusher-puller ($\beta_2 = \pm 1$) as a function of distance from the origin r along $\theta = \pi/2$, with various values of resistance δ. The Brinkman medium ($r > \lambda$) is shaded in gray; here $\lambda = 3$. The dash-dotted lines representing different algebraic decay scalings are shown for comparison.

line). In such a purely viscous medium, the flow around a neutral squirmer decays as $1/r^3$ (potential dipole), whereas the flow around a pusher-puller decays as $1/r^2$ (Stokes force dipole). The presence of a Brinkman medium surrounding the viscous region alters the rate of flow decay differently for a neutral squirmer than a pusher-puller. For a neutral squirmer, while the presence of additional resistance in the Brinkman medium further reduces the magnitude of flow in the far field, the decay rate remains the same in the Brinkman medium as $1/r^3$ in the Stokes case. In contrast, the flow around a pusher-puller decays much more rapidly as $1/r^4$ in the Brinkman medium than in the Stokes case ($1/r^2$). In the limit $\lambda = 1$, the swimmers are immersed in a Brinkman medium without the presence of a purely viscous regime and the rates of flow decay remain the same as $1/r^3$ for a neutral squirmer and $1/r^4$ for a pusher-puller [77].

Next we consider the energetic cost of swimming. Since the work done by the surface squirming motion is equal to the power dissipation in the fluid, we calculate the power $\mathcal{P}$ as

$$\mathcal{P} = -\int \mathbf{T}_N \cdot \mathbf{n} \cdot \mathbf{u}\, dS. \tag{24}$$

Upon calculating the surface integral using the flow field given by Eqs. (15)–(17), the power dissipation for a neutral squirmer is given by

$$\mathcal{P} = \frac{16\pi}{3}\left[1 + \frac{\delta^2(1+\lambda\delta)}{2\mathcal{B}}\right], \tag{25}$$

where $\mathcal{B}$ is given by Eq. (23). The expression for a two-mode squirmer can be obtained in the same manner. We reduce the above result to previously known limits. In the limit $\delta = 0$ (or $\lambda \to \infty$), we recover the power dissipation in a purely viscous medium [9,10], $\mathcal{P}_S = 16\pi/3$. In the other limit $\lambda = 1$, we obtain the power dissipation in a Brinkman medium [77], $\mathcal{P}_B = 8\pi(18 + 18\delta + 3\delta^2 + \delta^3)/3(9 + 9\delta + \delta^2)$.

As a remark, the power dissipation of a swimmer in the degelled region falls between $\mathcal{P}_S < \mathcal{P} < \mathcal{P}_B$ for any resistance $\delta > 0$ and size of the degelled region $\lambda > 1$. It is straightforward to show that $\partial\mathcal{P}/\partial\lambda < 0$, so the power dissipation monotonically decreases from the Brinkman limit $\mathcal{P}_B$ to the Stokes limit $\mathcal{P}_S$ as the size of the degelled region λ increases from unity towards infinity.

IV. CONCLUDING REMARKS

In this work, we use a spherical squirmer as a generic locomotion model to investigate its swimming characteristics in a viscous fluid surrounded by a Brinkman medium. The setup represents a minimal model for the hypothesized strategy employed by bacteria *H. pylori* or artificial microswimmers to enhance locomotion by liquifying their surrounding mucus gel. By modeling the liquefied region as a viscous fluid and the mucus gel as a Brinkman medium, the current model possesses swimming characteristics consistent with the hypothesis. In particular, for a squirmer with tangential surface velocities, we have revealed the existence of a minimum threshold size of mucus gel that a swimmer needs to liquify in order to gain any enhancement in propulsion speed. We have also demonstrated that these characteristics can vary significantly depending on the details of surface velocities; a squirmer with radial surface velocities displays qualitatively different characteristics. These different characteristics lead to interesting implications in terms of understanding the strategy bacteria *H. pylori* employe to invade biological barriers and the design of artificial microswimmers to perform the same function for more effective drug delivery.

We remark on the limitations and future direction of the current work. As a model for the enhanced locomotion by degelation, we assume the presence of the degelled region *a priori* and consider only the hydrodynamic problem in this work; namely, we investigate how the swimming performance depends on the size of the degelled region and fluid properties. For a more complete model, as sketched out by Mirbagheri and Fu [29], the hydrodynamic problem should be coupled to the mass transport problem of ammonia generated by the swimmer. The coupling between the two problems allows the determination of self-consistent values of swimming speed and size of the degelled region. Building on the pioneering work by Mirbagheri and Fu [29], the analytical solution based on a spherical squirmer in this work can be utilized in

conjunction with the advection-diffusion problem by Acrivos and Taylor [84] to construct a more geometrically consistent model for the degelation process. Analysis along this direction is currently under way and will be reported in a future work.

ACKNOWLEDGMENTS

O.S.P. was partially supported by the National Science Foundation under Grants No. EFMA-1830958 and No. CBET-1931292. H.N. acknowledges support from the John J. and Char Kopchick College of Natural Sciences and Mathematics at Indiana University of Pennsylvania.

APPENDIX A: SQUIRMING WITH RADIAL SURFACE VELOCITIES

Although squirmers with tangential surface velocities are more commonly studied in the literature [11], we present results on squirming with radial surface velocities in this Appendix for completeness. Following the formulation by Lighthill and Blake [9,10], the radial surface velocities on a squirmer ($r = a$) can be expressed in dimensional form as

$$\mathbf{u}_{sq} = \sum_{n=1}^{\infty} A_n P_n(\cos\theta)\mathbf{e}_r, \tag{A1}$$

where A_n and $P_n(\cos\theta)$ represent, respectively, a radial mode of surface velocity and a Legendre polynomial. Following the same solution method outlined previously but with the boundary condition for radial surface velocity given in Eq. (A1), we obtain the propulsion speed

$$U = -\left[\frac{1}{3} + \frac{2\delta^2}{\mathcal{B}} + \frac{\delta^2(\lambda^2-1)(3+\lambda\delta)}{\mathcal{B}}\right]A_1, \tag{A2}$$

where $\mathcal{B}$ is given by Eq. (23). In the limit of $\delta = 0$ (or $\lambda \to \infty$), we recover the results in Stokes flow [9,10], i.e., $U = -A_1/3$. In the limit $\lambda = 1$, we recover the results in Brinkman flow [73], $U = -(3+3\delta+\delta^2)A_1/(9+9\delta+\delta^2)$.

Our results on propulsion speed for $\lambda > 1$ and $\delta > 0$ are shown in Fig. 3. In contrast to the case with tangential surface velocities [Fig. 2(a)], local maxima in propulsion speed occurs as the size of the degelled region increases, leading to different biological implications, as discussed in Sec. III A.

APPENDIX B: COEFFICIENTS IN THE FLOW FIELDS

The expressions for coefficients O_n, Q_n, R_n, and S_n for $n = 1, 2$ in Eqs. (15)–(20) are given in this Appendix. The coefficients associated with the B_1 mode are given by

$$O_1 = \frac{1}{C_1}[6\delta^3\lambda - 2\delta^3\lambda^3 - 4\delta^3 - 6\delta^2\lambda^2 + 6\delta^2 + (3\delta^3\lambda^3 - 3\delta^3\lambda + 9\delta^2\lambda^2 - 3\delta^2)U], \tag{B1}$$

$$Q_1 = \frac{1}{C_1}[6\delta^3\lambda^5 - 10\delta^3\lambda^3 + 4\delta^3 + 30\delta^2\lambda^4 - 30\delta^2\lambda^2 + 120\delta\lambda^3 + (9\delta^2 - 4\delta^3\lambda^6 - 5\delta^3\lambda^3 + 9\delta^3\lambda - 24\delta^2\lambda^5 - 15\delta^2\lambda^2 - 180\delta\lambda^4 - 180\lambda^3)U], \tag{B2}$$

$$R_1 = \frac{1}{C_1}[10\delta^3\lambda^3 - 4\delta^3\lambda^6 - 6\delta^3\lambda - 24\delta^2\lambda^5 + 30\delta^2\lambda^2 - 6\delta^2 - 180\delta\lambda^4 - 180\lambda^3 + (6\delta^3\lambda^6 - 6\delta^3\lambda + 36\delta^2\lambda^5 - 6\delta^2 + 270\delta\lambda^4 + 270\lambda^3)U], \tag{B3}$$

$$S_1 = \frac{1}{C_1}[4\delta^3\lambda^6 - 6\delta^3\lambda^5 + 2\delta^3\lambda^3 + 24\delta^2\lambda^5 - 30\delta^2\lambda^4 + 6\delta^2\lambda^2 + 180\delta\lambda^4 - 120\delta\lambda^3 + 180\lambda^3 + (2\delta^3\lambda^3 - 2\delta^3\lambda^6 - 12\delta^2\lambda^5 + 6\delta^2\lambda^2 - 90\delta\lambda^4 - 90\lambda^3)U], \tag{B4}$$

$$T_1 = \frac{1}{\delta^2 C_1}[60\delta^3\lambda^4 - 24\delta^3\lambda^6 - 30\delta^3\lambda^3 - 6\delta^3\lambda - 84\delta^2\lambda^5 + 60\delta^2\lambda^3 + 30\delta^2\lambda^2 - 6\delta^2 - 180\delta\lambda^4 - 180\lambda^3 + (36\delta^3\lambda^6 - 30\delta^3\lambda^4 - 6\delta^3\lambda + 126\delta^2\lambda^5 - 30\delta^2\lambda^3 - 6\delta^2 + 270\delta\lambda^4 + 270\lambda^3)U], \tag{B5}$$

$$W_1 = \frac{e^{\delta\lambda}}{C_1}\sqrt{\frac{2\delta}{\pi}}[30\delta^3\lambda^3 - 6\delta^3\lambda^5 - 30\delta^3\lambda^2 + 6\delta^3 + 180\delta\lambda^3 + (9\delta^3\lambda^5 - 15\delta^3\lambda^3 + 6\delta^3 - 270\delta\lambda^3)U], \tag{B6}$$

$$C_1 = 4\delta^3\lambda^6 - 9\delta^3\lambda^5 + 10\delta^3\lambda^3 - 9\delta^3\lambda + 4\delta^3 + 24\delta^2\lambda^5 - 45\delta^2\lambda^4 + 30\delta^2\lambda^2 - 9\delta^2 + 180\delta\lambda^4 - 180\delta\lambda^3 + 180\lambda^3. \tag{B7}$$

The coefficients associated with the B_2 mode read

$$O_2 = \frac{1}{C_2}(10\delta^4\lambda^3 - 6\delta^4\lambda^5 - 4\delta^4 - 30\delta^3\lambda^4 + 30\delta^3\lambda^2 - 30\delta^2\lambda^3 + 30\delta^2\lambda), \tag{B8}$$

$$Q_2 = \frac{1}{C_2}(10\delta^4\lambda^7 - 14\delta^4\lambda^5 + 4\delta^4 + 70\delta^3\lambda^6 - 70\delta^3\lambda^4 + 210\delta^2\lambda^5 - 70\delta^2\lambda^3), \tag{B9}$$

$$R_2 = \frac{1}{C_2}(14\delta^4\lambda^5 - 4\delta^4\lambda^{10} - 10\delta^4\lambda^3 - 40\delta^3\lambda^9 + 70\delta^3\lambda^4 - 30\delta^3\lambda^2 - 390\delta^2\lambda^8 + 70\delta^2\lambda^3 - 30\delta^2\lambda - 1050\delta\lambda^7 - 1050\lambda^6), \tag{B10}$$

$$S_2 = \frac{1}{C_2}(4\delta^4\lambda^{10} - 10\delta^4\lambda^7 + 6\delta^4\lambda^5 + 40\delta^3\lambda^9 - 70\delta^3\lambda^6 + 30\delta^3\lambda^4 + 390\delta^2\lambda^8 - 210\delta^2\lambda^5 + 30\delta^2\lambda^3 + 1050\delta\lambda^7 + 1050\lambda^6), \tag{B11}$$

$$T_2 = \frac{1}{\delta^2 C_2}(105\delta^4\lambda^8 - 75\delta^4\lambda^{10} - 30\delta^4\lambda^3 - 435\delta^3\lambda^9 + 315\delta^3\lambda^7 + 210\delta^3\lambda^4 - 90\delta^3\lambda^2 - 1485\delta^2\lambda^8 + 315\delta^2\lambda^6 + 210\delta^2\lambda^3 - 90\delta^2\lambda - 3150\delta\lambda^7 - 3150\lambda^6), \tag{B12}$$

$$W_2 = \frac{e^{\delta\lambda}}{C_2}\sqrt{\frac{2\delta}{\pi}}(70\delta^4\lambda^6 - 30\delta^4\lambda^8 - 70\delta^4\lambda^3 + 30\delta^4\lambda + 1050\delta^2\lambda^6), \tag{B13}$$

$$C_2 = 4\delta^4\lambda^{10} - 25\delta^4\lambda^7 + 42\delta^4\lambda^5 - 25\delta^4\lambda^3 + 4\delta^4 + 40\delta^3\lambda^9 - 175\delta^3\lambda^6 + 210\delta^3\lambda^4 - 75\delta^3\lambda^2 + 390\delta^2\lambda^8 - 525\delta^2\lambda^5 + 210\delta^2\lambda^3 - 75\delta^2\lambda + 1050\delta\lambda^7 + 1050\lambda^6. \tag{B14}$$

[1] L. J. Fauci and R. Dillon, Annu. Rev. Fluid Mech. **38**, 371 (2006).
[2] H. Berg, *Random Walks in Biology* (Princeton University Press, Princeton, NJ, 1993).
[3] E. Lauga, Annu. Rev. Fluid Mech. **48**, 105 (2016).
[4] C. Brennen and H. Winet, Annu. Rev. Fluid Mech. **9**, 339 (1977).
[5] E. Lauga and T. R. Powers, Rep. Prog. Phys. **72**, 096601 (2009).
[6] R. E. Goldstein, Annu. Rev. Fluid Mech. **47**, 343 (2015).
[7] A. T. Chwang, T. Y. Wu, and J. Gray, Proc. R. Soc. B **178**, 327 (1971).
[8] G. Taylor, Proc. R. Soc. London, Ser. A **209**, 447 (1951).
[9] M. J. Lighthill, Commun. Pure Appl. Math. **5**, 109 (1952).
[10] J. R. Blake, J. Fluid Mech. **46**, 199 (1971).
[11] T. J. Pedley, IMA J. Appl. Math. **81**, 488 (2016).
[12] J. M. Yeomans, D. O. Pushkin, and H. Shum, Eur. Phys. J.: Spec. Top. **223**, 1771 (2014).
[13] J. Elgeti, R. G. Winkler, and G. Gompper, Rep. Prog. Phys. **78**, 056601 (2015).
[14] O. S. Pak and E. Lauga, *Fluid-Structure Interactions in Low-Reynolds-Number Flows* (Royal Society of Chemistry, Cambridge, UK, 2016), pp. 100–167.
[15] J. J. Abbott, K. E. Peyer, M. C. Lagomarsino, L. Zhang, L. Dong, I. K. Kaliakatsos, and B. J. Nelson, Int. J. Robot. Res. **28**, 1434 (2009).
[16] S. J. Ebbens and J. R. Howse, Soft Matter **6**, 726 (2010).
[17] S. Sengupta, M. E. Ibele, and A. Sen, Angew Chem. Int. Ed. **51**, 8434 (2012).
[18] C. Hu, S. Pané, and B. J. Nelson, Annu. Rev. Contr. Robo. Auto. **1**, 53 (2018).
[19] B. J. Nelson, I. K. Kaliakatsos, and J. J. Abbott, Annu. Rev. Biomed. Eng. **12**, 55 (2010).
[20] W. Gao, D. Kagan, O. S. Pak, C. Clawson, S. Campuzano, E. Chuluun-Erdene, E. Shipton, E. E. Fullerton, L. Zhang, E. Lauga, and J. Wang, Small **8**, 460 (2012).
[21] A. C. H. Tsang, E. Demir, Y. Ding, and O. S. Pak, Adv. Intell. Sys. (2020) 1900137, doi:10.1002/aisy.201900137.
[22] V. A. Martinez, J. Schwarz-Linek, M. Reufer, L. G. Wilson, A. N. Morozov, and W. C. K. Poon, Proc. Natl. Acad. Sci. USA **111**, 17771 (2014).
[23] J. P. Celli, B. S. Turner, A. N. H., S. Keates, I. Ghiran, C. P. Kelly, R. H. Ewoldt, G. H. McKinley, P. So, S. Erramilli, and R. Bansil, Proc. Natl. Acad. Sci. USA **106**, 14321 (2009).
[24] R. Bansil, J. P. Celli, J. M. Hardcastle, and B. S. Turner, Front. Immunol. **4**, 310 (2013).
[25] G. C. Hansson, Curr. Opin. Microbiol. **15**, 57 (2012).
[26] L. M. Brown, Epidemiol. Rev. **22**, 283 (2000).
[27] M. F. Go, Aliment. Pharm. Ther. **16**, 3 (2002).
[28] D. Walker, B. T. Käsdorf, H. H. Jeong, O. Lieleg, and P. Fischer, Sci. Adv. **1**, e1500501 (2015).
[29] S. A. Mirbagheri and H. C. Fu, Phys. Rev. Lett. **116**, 198101 (2016).
[30] S. Y. Reigh and E. Lauga, Phys. Rev. Fluids **2**, 093101 (2017).
[31] V. Magar, T. Goto, and T. J. Pedley, Q. J. Mech. Appl. Math. **56**, 65 (2003).
[32] S. Michelin and E. Lauga, Phys. Fluids **23**, 101901 (2011).
[33] S. Michelin and E. Lauga, J. Fluid Mech. **715**, 1 (2013).
[34] K. Shoele and P. S. Eastham, Phys. Rev. Fluids **3**, 043101 (2018).
[35] A. Zöttl and H. Stark, Phys. Rev. Lett. **108**, 218104 (2012).
[36] K. Ishimoto and E. A. Gaffney, Phys. Rev. E **88**, 062702 (2013).
[37] L. Zhu, E. Lauga, and L. Brandt, J. Fluid Mech. **726**, 285 (2013).
[38] G.-J. Li and A. M. Ardekani, Phys. Rev. E **90**, 013010 (2014).
[39] K. Schaar, A. Zöttl, and H. Stark, Phys. Rev. Lett. **115**, 038101 (2015).
[40] F. Ruhle, J. Blaschke, J.-T. Kuhr, and H. Stark, New J. Phys. **20**, 025003 (2018).
[41] T. Ishikawa and K. Kikuchi, Proc. R. Soc. B **285**, 20172368 (2018).
[42] T. Ishikawa, J. Appl. Phys. **125**, 200901 (2019).
[43] B. Felderhof and R. Jones, Phys. A (Amsterdam, Neth.) **202**, 119 (1994).
[44] S. Wang and A. Ardekani, Phys. Fluids **24**, 101902 (2012).
[45] N. G. Chisholm, D. Legendre, E. Lauga, and A. S. Khair, J. Fluid Mech. **796**, 233 (2016).
[46] L. Zhu, M. Do-Quang, E. Lauga, and L. Brandt, Phys. Rev. E **83**, 011901 (2011).
[47] L. Zhu, E. Lauga, and L. Brandt, Phys. Fluids **24**, 051902 (2012).

[48] G. J. Li, A. Karimi, and A. M. Ardekani, Rheol. Acta **53**, 911 (2014).
[49] S. Yazdi, A. M. Ardekani, and A. Borhan, Phys. Rev. E **90**, 043002 (2014).
[50] M. De Corato, F. Greco, and P. L. Maffettone, Phys. Rev. E **92**, 053008 (2015).
[51] M. De Corato and G. D'Avino, Soft Matter **13**, 196 (2017).
[52] C. Datt, L. Zhu, G. J. Elfring, and O. S. Pak, J. Fluid Mech. **784**, R1 (2015).
[53] H. Nganguia, K. Pietrzyk, and O. S. Pak, Phys. Rev. E **96**, 062606 (2017).
[54] C. Datt, G. Natale, S. G. Hatzikiriakos, and G. J. Elfring, J. Fluid Mech. **823**, 675 (2017).
[55] K. Pietrzyk, H. Nganguia, C. Datt, L. Zhu, G. J. Elfring, and O. S. Pak, J. Non-Newtonian Fluid Mech. **268**, 101 (2019).
[56] K. Qi, E. Westphal, G. Gompper, and R. G. Winkler, Phys. Rev. Lett. **124**, 068001 (2020).
[57] T. Ishikawa, M. P. Simmonds, and T. J. Pedley, J. Fluid Mech. **568**, 119 (2006).
[58] T. Ishikawa and T. J. Pedley, Phys. Rev. Lett. **100**, 088103 (2008).
[59] A. Zöttl and H. Stark, Phys. Rev. Lett. **112**, 118101 (2014).
[60] B. Delmotte, E. E. Keaveny, F. Plouraboue, and E. Climent, J. Comput. Phys. **302**, 524 (2015).
[61] J. Blaschke, M. Maurer, K. Menon, A. Zottl, and H. Stark, Soft Matter **12**, 9821 (2016).
[62] J.-T. Kuhr, F. Rühle, and H. Stark, Soft Matter **15**, 5685 (2019).
[63] A. Doostmohammadi, R. Stocker, and A. M. Ardekani, Proc. Natl. Acad. Sci. USA **109**, 3856 (2012).
[64] T. J. Pedley, D. R. Brumley, and R. E. Goldstein, J. Fluid Mech. **798**, 165 (2016).
[65] B. U. Felderhof and R. B. Jones, Phys. Fluids **28**, 073601 (2016).
[66] C. Datt and G. J. Elfring, Phys. Rev. Lett. **123**, 158006 (2019).
[67] H. C. Brinkman, Appl. Sci. Res. **1**, 27 (1949).
[68] C. K. W. Tam, J. Fluid Mech. **38**, 537 (1969).
[69] S. Childress, J. Chem. Phys. **56**, 2527 (1972).
[70] I. D. Howells, J. Fluid Mech. **64**, 449 (1974).
[71] E. J. Hinch, J. Fluid Mech. **83**, 695 (1977).
[72] L. Durlofsky and J. F. Brady, Phys. Fluids **30**, 3329 (1987).
[73] A. M. Leshansky, Phys. Rev. E **80**, 051911 (2009).
[74] S. Jung, Phys. Fluids **22**, 031903 (2010).
[75] N. Ho, S. D. Olson, and K. Leiderman, Phys. Rev. E **93**, 043108 (2016).
[76] K. Leiderman and S. D. Olson, Phys. Fluids **28**, 021902 (2016).
[77] H. Nganguia and O. S. Pak, J. Fluid Mech. **855**, 554 (2018).
[78] N. Ho, K. Leiderman, and S. Olson, J. Fluid Mech. **864**, 1088 (2019).
[79] J. Higdon and M. Kojima, Int. J. Multiphase Flow **7**, 719 (1981).
[80] R. H. Davis and H. A. Stone, Chem. Eng. Sci. **48**, 3993 (1993).
[81] O. S. Pak and E. Lauga, J. Eng. Math. **88**, 1 (2014).
[82] T. Zlatanovski, Q. J. Mech. Appl. Math. **52**, 111 (1999).
[83] D. Palaniappan, J. Theor. Appl. Mech. **52**, 405 (2014).
[84] A. Acrivos and T. D. Taylor, Phys. Fluids **5**, 387 (1962).